Master's Thesis
석사 학위논문

Continuum Flexible Robot with Multiple Curvature

Bak Seongho(박 성 호 朴 成 鎬)

Department of Robotics Engineering

로봇공학전공

DGIST

2016

Master's Thesis
석사 학위논문

Continuum Flexible Robot with Multiple Curvature

Bak Seongho(박 성 호 朴 成 鎬)

Department of Robotics Engineering

로봇공학전공

DGIST

2016

Continuum Flexible Robot with Multiple Curvature

Advisor : Professor Jaesung Hong

Co-advisor : Professor Sanghyun Joung

by

Bak Seongho

Department of Robotics Engineering

DGIST

A thesis submitted to the faculty of DGIST in partial fulfillment of the requirements for the degree of Master of Science. The study was conducted in accordance with Code of Research Ethics[1]

07. 06. 2016

Approved by

Professor Jaesung Hong (_____)

(Advisor)

Professor Sanghyun Joung (_____)

(Co-Advisor)

[1] Declaration of Ethical Conduct in Research: I, as a graduate student of DGIST, hereby declare that I have not committed any acts that may damage the credibility of my research. These include, but are not limited to: falsification, thesis written by someone else, distortion of research findings or plagiarism. I affirm that my thesis contains honest conclusions based on my own careful research under the guidance of my thesis advisor.

Continuum Flexible Robot with Multiple Curvature

Bak Seongho

Accepted in partial fulfillment of the requirements for the degree of Master of Science.

06. 01. 2016

Head of Committee	Professor Jaesung Hong	(인)
Committee Member	Professor Sanghyun Joung	(인)
Committee Member	Professor Cheol Song	(인)

MS/RT

201423008

박 □ □. Bak Seongho. The study of continuum flexible robot with multiple curvature. Department of Robotics Engineering. 2016. 34p.

Advisors Prof. Jaesung Hong, Co-Advisors Prof. Sanghyun Joung.

ABSTRACT

The continuum flexible robots are used at various fields due to characteristics of relatively more flexible than conventional rigid link-joint robots. Among many applications, this paper researches of the continuum flexible robot which can be apply with ballooning orbital floor blowout surgery. When the balloon support the fracture under the fractured orbital floor, the completeness of the surgery grows though this procedure can be performed by highly trained few surgeons. The core problem is the tip of the robot should bend most to get into the side pathway in narrow space by 1-DOF. The conventional flexible robots suppose it has equal curvature in entire flexible part or are got restrict of their structures for constant curvatures. For supplementing those problems, this paper designed the continuum flexible robot which has larger curvatures at the tip without increasing the number of actuators and analyzed the curvature ratio, the curvature according to the length of pulled wires and kinematics. The continuum flexible robot was tested by pulled wire from $0mm$ to $15mm$ and then was compared with measured value and estimated value.

Keywords: continuum flexible robot, curvature, curvature ratio, kinematics

Contents

List of contents

List of Tables

List of Figures

I. INTRODUCTION

1.1 Orbital floor blowout

Orbital floor blowout frequently occur after blunt trauma to the face. Typical symptoms of an inferior orbital blowout are enophthalmos, limited eye movement, and diplopia which are explained by Figure 1 [1-4]. Surgical approaches have been used to reconstruct orbital fractures. Surgeons should replace orbital contents and support the bones while restoring orbital volume and shape [2]. Doctors check movement of eyes, eyesight test, diplopia (double vision). In addition, patients are usually scanned by computer tomograph (CT). The surgeon usually operate few days after injured when the edema is fell out which is caused by trauma.

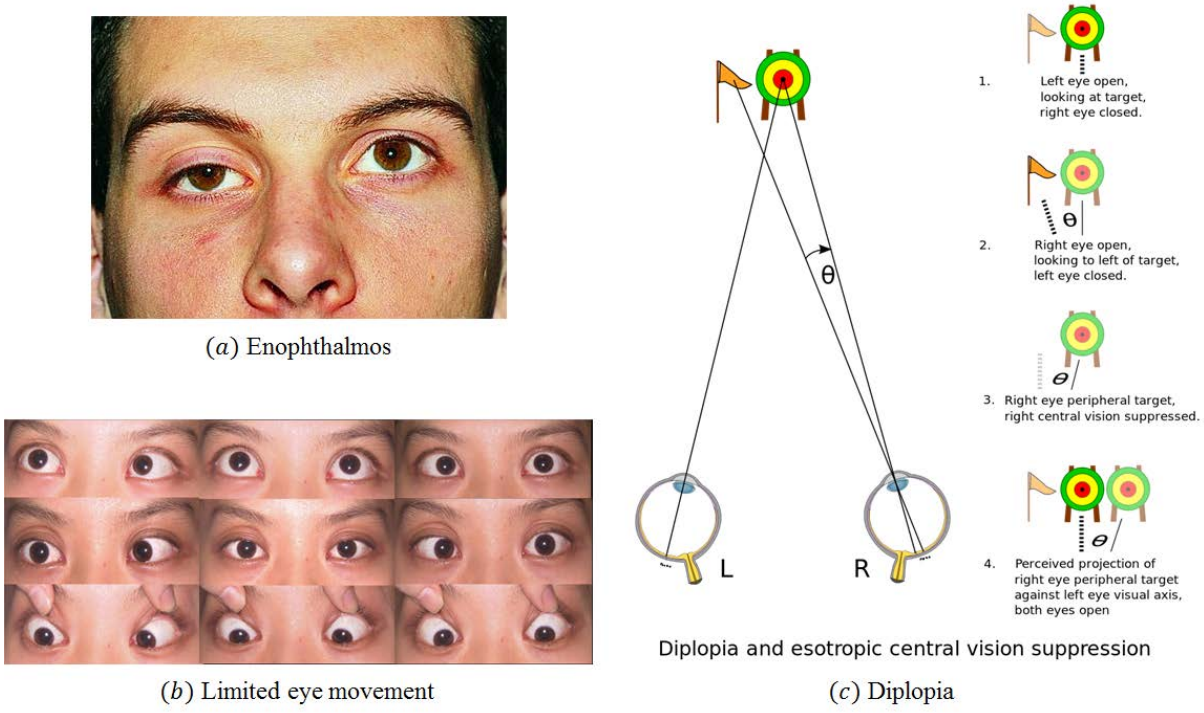

Figure 1. The explanation of typical symptom of an inferior orbital blowout.

Conventional orbital floor blowout surgery is a direct transconjunctival approach. After incision of under the eyelid which contains conjunctiva, the surgeon push aside the periosteum and eyeball then check the fracture position. The herniated orbital contents are repositioned into the original position through the fracture, and the

factures are removed. When an operating surgeon decide the volume of the eye socket is well reconstructed, the surgeon put an implant on the orbital floor. The eye ball finally release into original position then the surgery is finished. In this situation, when the surgeon wants to reposition the orbital contents, the limitation of the surgical tools are problem. Because picking out the orbital contents from sinus is uncomfortable and also has poor view due to the surgical fields surrounding. Deflection of implant also cannot guarantee of original orbital volume and it causes leave from original position of implant. The Figure 2 indicate brief description [5].

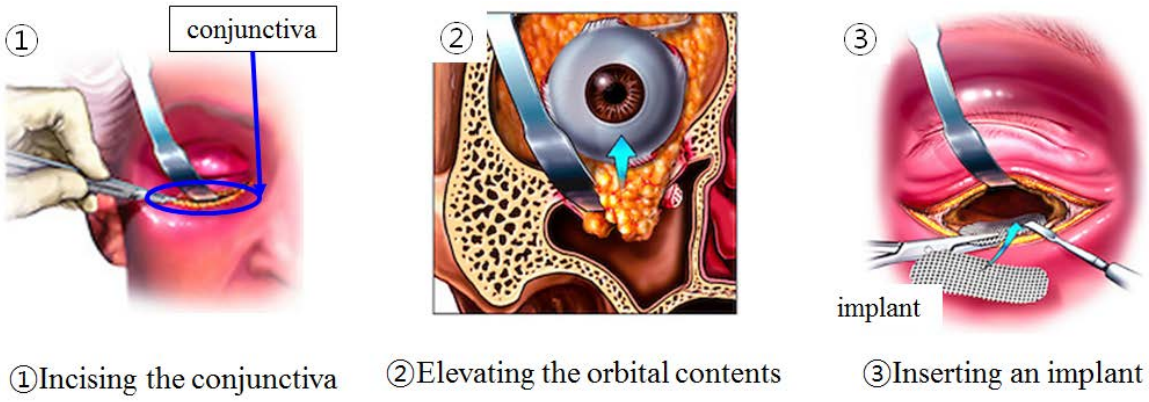

Figure 2. The conventional procedure of orbital floor blowout surgery.

N. K. Lim, D. H. Kang et al are suggested transnasal balloon technique because of foregoing method's problems [6]. In the suggested surgery, a surgeon inflate the balloon inside of maxillary sinus by transnasal approach. First of all, the patient lay down with one's head lower than body. After a surgeon check the fracture of orbital floor by eyelid approach, precurved Freer elevator is inserted into the maxillary sinus through the maxillary ostium which is a natural orifice. Then the bone fractures and herniated orbital contents are repositioned for recovering original volume and shape. When the reposition is over and Freer elevator is took out from the nose, a surgeon push the Foley catheter (which is about 30cc) with mosquito into the inside of maxillar sinus. The Foley catheter support the orbital contents under the orbital floor when it is ballooned and it is held about a week. The rest is applying implant over the fracture and finishing the surgery like conventional method. This method was demonstrated more effective for restoring. There are three problems about the previous method. The first problem is only highly skilled surgeons can operate this method because there is no space for endoscope. Only few surgeons can put a surgical instrument to the maxillary sinus through the maxillary ostium althogh the surgeons have to. The second problem is the precurved rigid surgical instruments make difficult to put the Freer elevator and balloon into the

maxillary sinus. Especially putting the balloon in to the maxillary sinus is hard even if a surgeon is skillful. The last problem is that the patients nose get stress during surgery. The patients nose usually distorted because of curved narrow space and rigid surgical tools. The Figure 3 shows the three problems.

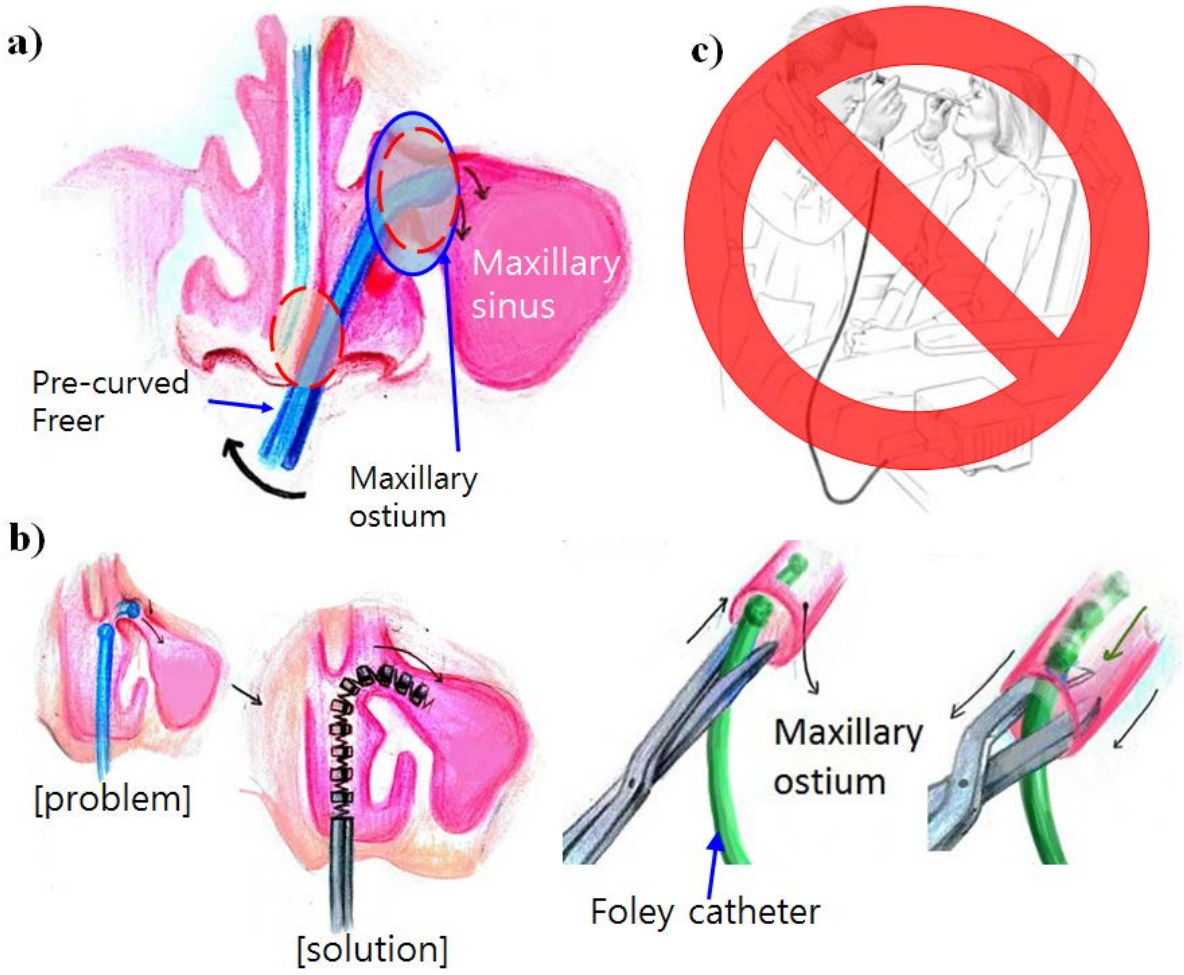

Figure 3. The three problems of the ballooning orbital floor blowout

1.2 Previous researches of the flexible robot

Many research groups have been developed flexible robot and evaluated due to its flexible movement. Until now, various type of the flexible robots are develop. Ian D. Walker et al. has been developed and analyzed their flexible robots which are actuated by wires or pneumatic compressor [7], [8], [9], [10]. They derived kinematics model and applied to their elephant's trunk manipulator. Also they intended the model can correspond to other continuum type robot. But the robot is too big to use for surgery. David B. Carmarillo et al. derived the mechanics model of tendon-driven continuum manipulators [11]. They analyzed it with beam configuration. The research group at

mechanical engineering department, University of Wisconsin-Madison considered the influence of friction between wires and catheter [12], [13]. William S. Rone and Pinhas Ben-Tzvi also analyzed the dynamics of continuum robot with utilizing the principle of virtual power [14]. Ceilia Laschi at el. developed soft robot arm which is actuated by SMAs [15]. But all of the prior introduced researches did not focused on not only multiple curvature when the robot moves by 1-DOF but also intended different curvatures. Except Ian D. Walker et al. and David B. Carmarillo et al., research groups also did not consider the relationship of curvature and length of compressed side. To use the flexible robot for medical device, the safety should be guaranteed. Hyun-Soo Yoon et al. developed the flexible robot for maxillary sinus surgery [16], [17]. It has basically safe mechanical structure due to using compression springs for backbone. But they did not consider of multiple curvature in 1-DOF movement. Zheng Li et al. used rigid vertebra spherical joint which has many DOFs [18], [19]. Also their robot can be controlled the curvature by two section by inserting constrained bar in the middle of flexible robot. But it has a limit of curvature due to using only rigid spherical joint and divide the curvature only two section. In this paper, we improve the dexterity of the flexible robot about having multiple curvatures and suggest the kinematics for the continuum flexible robot.

1.3 Research contents and goal

In this paper, the continuum flexible robot with multiple curvature which has larger curvature at the tip is presented. The design and kinematics analysis of the flexible robot is introduced then its prototype is shown. We designed the continuum flexible robot first then proposed kinematics model.

The continuum flexible robot is composed of three parts which are flexible part, actuation part and electronic devices. Flexible part consist of compression spring backbone and spring connecting cylinder. We can give variety for choosing springs section by section. The entire flow to achieve position information from the length of wire pulled is

$$l_{i,pull} \xrightarrow{f_1} c_p, c_d, \phi \xrightarrow{f_2} \theta_i, d \xrightarrow{f_{D-H}} x, y, z \quad (1)$$

and the ratio of curvature, $c_p : c_d$, was obtained by considering mechanical spring analysis. The function of entire relationships can be divided by three parts. The f_1 is main transformation function. It is the relationship from the pulled length of wire $l_{\mathrm{i,pull}}$ to curvature $c_p, \mathrm{c_d}$ and the angle of curvature ϕ. The f_1 is main contribution of

this research's theory. The f_2 express the relationship from $c_p, \mathrm{c_d}, \phi$ to θ_i, d. We made the rigid link and joint model about a single flexible part. It makes we can get the position data by the curvatures and the angle of curvature. Finally, we can get the position data of the continuum flexible robot through f_{D-H}. We evaluated the functions through making prototype and experiment the curvatures and positions. When we made prototype, the spring constant of first seventh springs are $4.9kN/mm$ and rest three springs are $0.49kN/mm$.

Our main contribution is finding relationships of curvature and spring constant and applying it to kinematics to get a position information. The first function, calculating proximal and distal curvatures and curvature formation angle from pulled wire length, was modified. Because of uncertainty of the wires outside length, we only consider the length of inner side. The detail explanation will be continued in section 3.1.3. The second function was achieved by geometrical approach based on rigid link-joint model. The third, we got a position information through Denavit–Hartenberg parameters. Finally, we comparing the curvatures and position information of estimated and measured value by experiments.

II. DESIGN

In this research, the continuum flexible robot has to have relatively large curvature at the distal part and limber backdrivability at a body. Because the robot can pass through the route of different curvature for each section like the route for reaching maxillary sinus. The Figure 4. shows the flexible robot formed by 3 part which are flexible part, driving part and electronic devices. The flexible part is attached to driving part with conduit. The driving part consist of three servo motors and other mechanical components. The electronic devices contain MCU(Arduino Due), communication transducer, power transformation, joystick and power supply. The robot has 3-DOF which has two orthogonal rotation and one translation. Users operate the robot by their own view feedback.

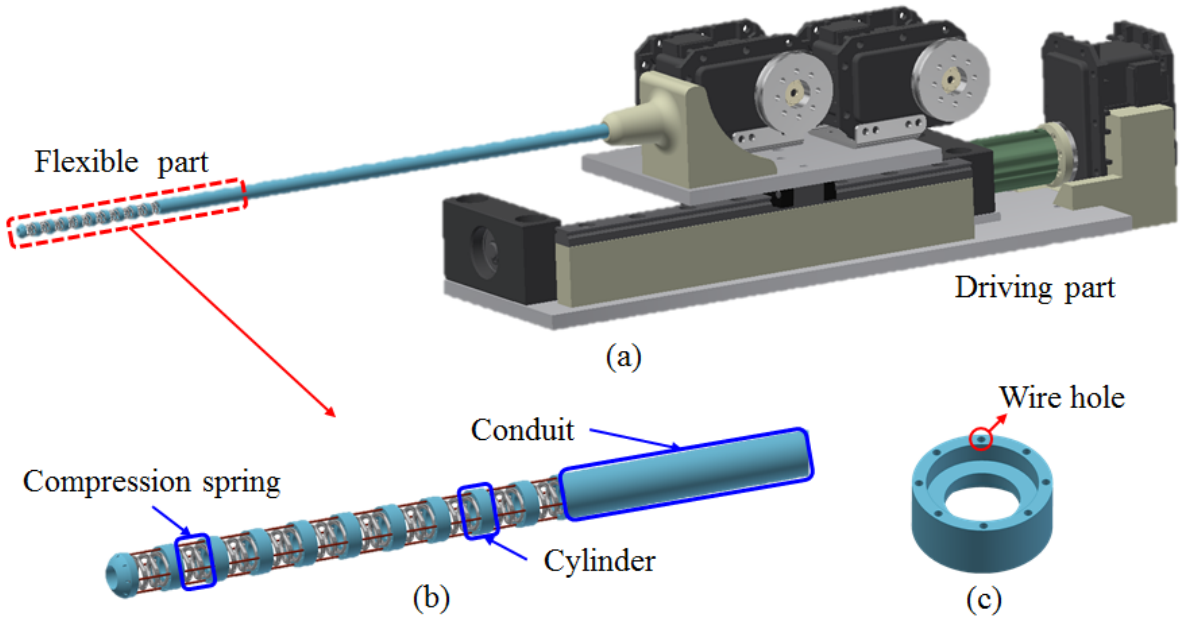

Figure 4. (a) The flexible part combined with driving part. (b) The three component of flexible part. (c) Detail view of cylinder in the flexible part.

2.1 Flexible part

The flexible part has three kind of spring connect cylinder and conduit which connect compression springs. Compression springs' outer diameter is $4mm$ and the outer diameter of cylinders and conduit are $5mm$.

Cylinders and conduit have $2.7mm$ hole in the center and eight $0.3mm$ hole for wire. Due to the center hole, the robot has 1 channel that can be used for endoscope or end-effector. 4 wires which are connected by pulley for each pair makes 2-DOF movement. Entire length of the flexible part is $63.012mm$ which is divided by proximal part of $42.409mm$ and distal part of $20.603mm$. The proximal part is divided by 7 segments which has $4.9N/mm$ for spring constant k_p. The distal part has 3 segments which has $0.49N/mm$ for spring constant k_d. The length of each single segment are 4.119mm and 3.735mm. They are distance between connecting cylinders s_d and s_p. The detail drawing of flexible part is shown in Figure 5.

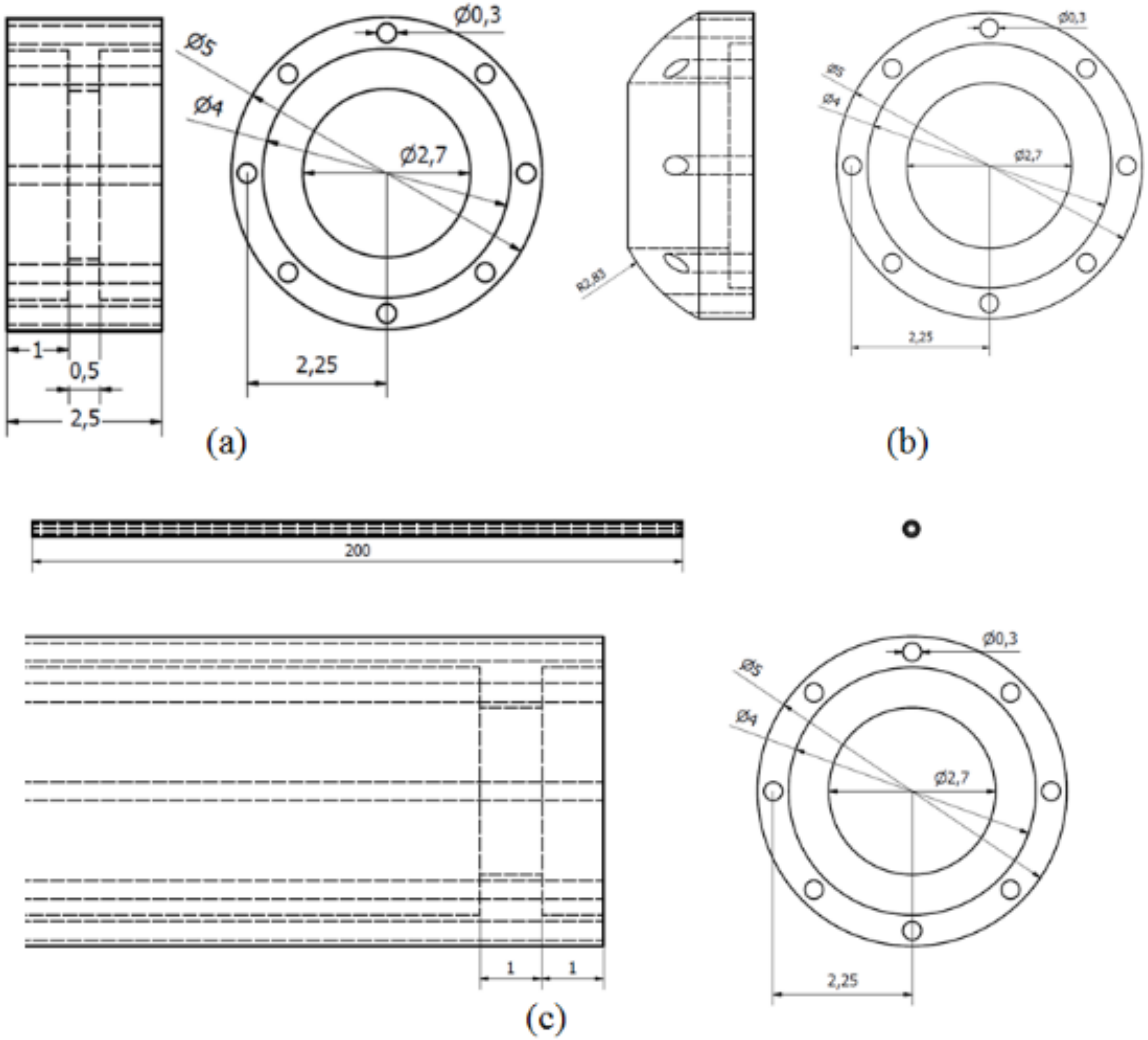

Figure 5. (a) The cylinder. (b) The end cap. (c) The conduit

2.2 Driving part

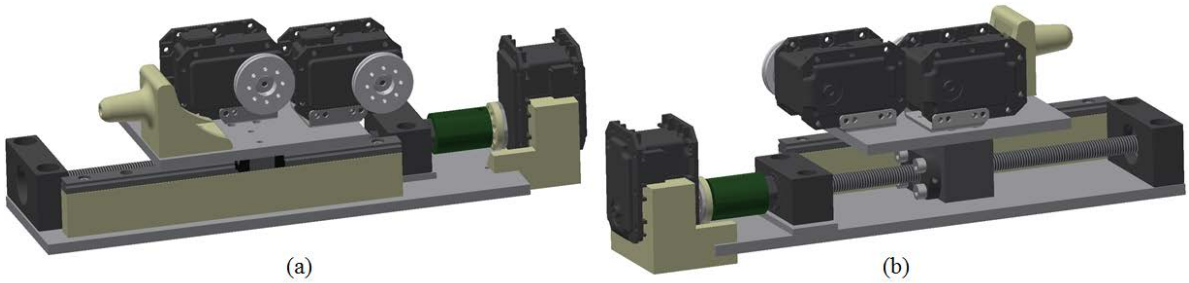

Figure 6. The view of driving part. (a) The front view. (b) The rear view.

The Figure 6 illustrate the driving part which consist of three servo motors (MX-28R, Robotis), two pulley at each motors that laid down on upper plate, $150mm$ ball screw, support unit, $150mm$ linear guide, coupling, aluminum plates. The holders for conduit and motor for rotating ball screw and support block for linear guide are made by 3D printer (Objet ADEN E250, Stratasys). Two pair of wires are twined around at pulley so they make total 2-DOF. Rest 1-DOF of translation is controlled by ball screw.

2.3 Electronic devices

For control three motors, 2-DOF joystick and two push switches are used. MCU (Arduino Due) convert the analog signal from joystick, MX485 chip convert USART from Arduino to RS485 which used by motors. The X, T rotation joystick controls each servo motor on the plate in Figure 6. The two push button controls the servo motor which is attached to ball screw for Z translation. The configuration of electronic devices are illustrated in Figure 7.

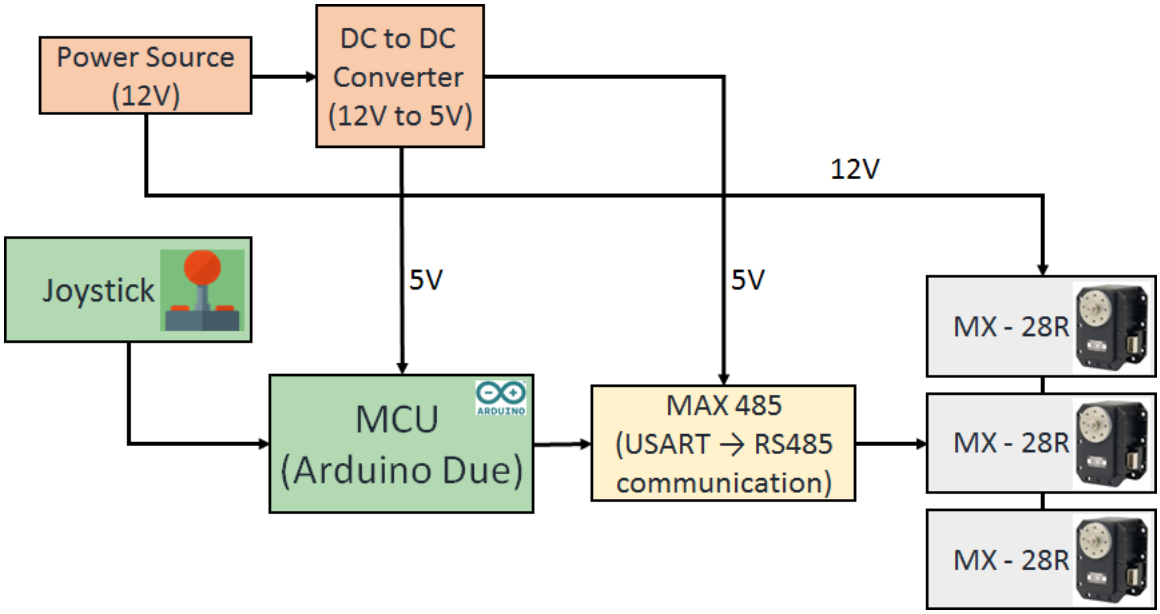

Figure 7. The configuration of electronic devices.

III. KINEMATICS ANALYSIS

3.1 Relationship between the length of pulled wire, curvature and angle of curvature

The first step of kinematics of the continuum flexible robot is knowing about the relationship between wire pulled length, $l_{i,pull}$ to curvature c_p, c_d and the angle of curvature ϕ. To find curvature, we have to know about the wire length of compressed side of spring l_i. We assume the outer arc length of spring is consistent which is opposite side of compressed side. We consider about relationship of curvature and spring constant because we use springs of different constant. Through the relationship of two curvature we can get wire length of compressed side at proximal and distal part. When the robot bend by two combination of wire, the angle of curvature ϕ should be considered. We have to combine relationships of $l_{i,pull}$ and c_p, c_d with ϕ then apply to conventional method of robotics.

3.1.1 Kinematics model of a single spring

The curvature changes depending on wire length of compressed side. First we have to know the relationship between wire length and curvature. We adjust the law of cosine to the Figure 8 and suppose the outer line is neutral line. The wire length is $\frac{l_i}{\mathrm{n}} = \sqrt{2\left(\frac{1}{c} - 2r\right)^2 - 2\left(\frac{1}{c} - 2r\right)^2 \cos\theta}$. After rearranging the equation and substitute $\theta = \frac{cs}{n}$, we can get

$$l_i = 2n\left(\frac{1}{c} - 2r\right)\sin\frac{cs}{2n} \tag{1}$$

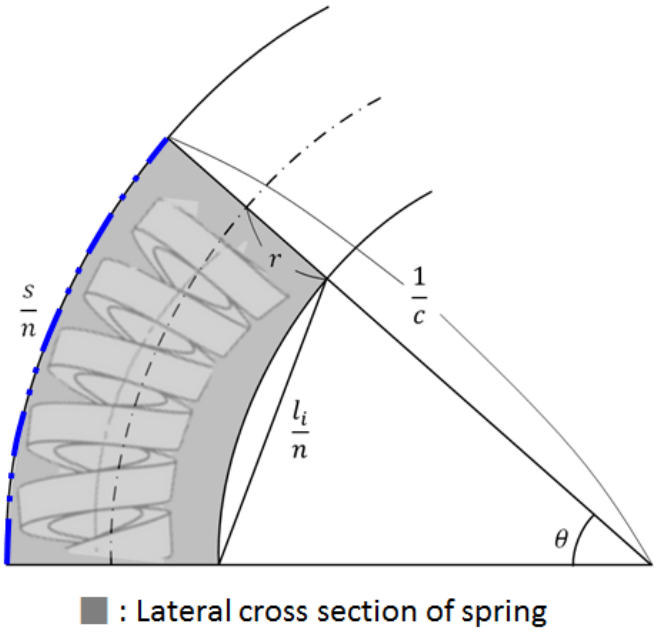

Figure 8. The lateral view of a single spring section at the flexible part when only a wire was pulled.

3.1.2 Stress analysis and relationship of the spring constant k and the curvature of a spring c

In this paper, we use springs which has several different spring constant. To get a relationship of the spring constant and the curvature of a spring, we have to analyze the stress of cross section of spring coil. The analysis of compression helical spring was explained at [20]. We applied conventional method to analyze the spring.. In Figure 9, the shear stress which is away from center O with ρ is $\tau = \frac{\tau_m}{\frac{d}{2}}\rho$. In here, d is diameter of compression spring and τ_m is maximum shear stress. The moment of shaded ring which has radius ρ and width $d\rho$ is $dM = 2\pi\rho^2 d\rho\tau$. In here, ρ is distance to points of action, $2\pi\rho d\rho$ is the area where the shear stress is applied. In Figure 10, the total torque moment is $FD = \int_0^{\frac{d}{2}} dM = \int_0^{\frac{d}{2}} \frac{4\pi\tau_m\rho}{d} d\rho = \frac{\pi d^3 \tau_m}{16}$ when compression spring bend to one side. So the maximum shear stress is

$$\tau_m = \frac{16FD}{\pi d^3}. \tag{2}$$

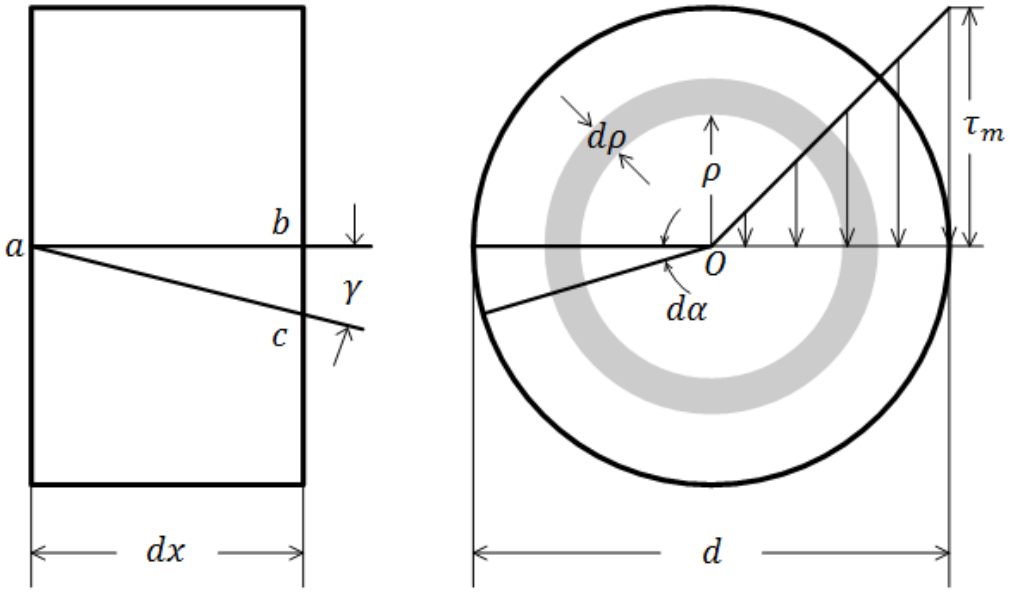

Figure 9. The shear stress of cross-sectional element of spring coil

By elastic theory, distortion angle is achieved by $\gamma = \frac{\tau_m}{G} = \frac{16FD}{\pi d^3 G}$. In here, *G* is the shearing modulus of elasticity. As we can see in Figure 9, distortion angle is $d\alpha = \frac{\gamma dx}{d/2}$ due to $\overline{bc} = \gamma dx$. In [20], the text book demonstrated the entire deflection angle β by When the spring is considered to straight bar, entire deflection angle β of one side of bar can be achieved by integrating $d\alpha$ from *0* to πnr. It is $\beta = \int_0^{\pi nr} d\alpha = \int_0^{\pi nr} \frac{2\gamma}{d} dx = \int_0^{\pi nr} \frac{32FD}{\pi d^4 G} dx = \frac{16FD^2 n}{d^4 G}$. So the deflection angle θ of a single spring is

$$\theta = \beta = \frac{2F}{Dk}. \tag{3}$$

In here, $k = \frac{d^4 G}{8D^3 n}$ is spring constant of compression spring. Substituting $\theta = sc$ to (3) due to Figure 11, we can achieve the relationship between curvature and spring constant

$$c = \frac{2F}{sD} \cdot \frac{1}{k}. \tag{4}$$

So when the different springs which have same outer diameter are connected, the relationship of curvature and spring constant is

$$\frac{c_1}{c_2} = \frac{k_2}{k_1}. \tag{5}$$

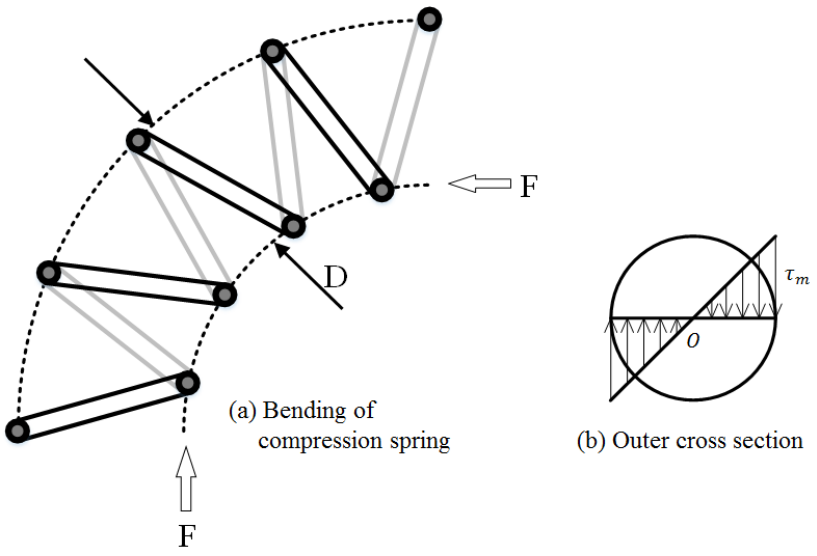

Figure 10. (a) The bending of compression spring. (b) The shear stress at cross section.

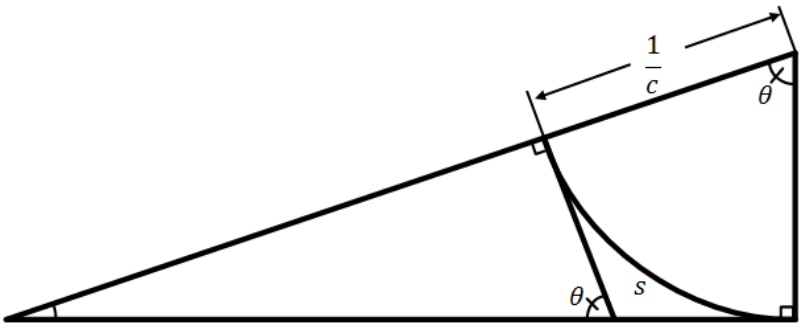

Figure 11. The relation between curvature and deflection angle.

3.1.3 Wire length of the compressed part of spring in proximal part $l_{i,p}$ and distal part $l_{i,d}$

The continuum flexible robot of this paper has different tendency in shape of curvature. The flexible robot of this research has large curvature at the distal part. It means the wire length of the compressed part of spring in proximal part and distal part. To calculate the wire length of compressed part of spring for designed flexible robot, we have to divide the section according to sort of the springs. In this case, the meaningful curvature increase until

0.16. Because of the range of κ from 0 to 0.16, $l_i = 2n\left(\frac{1}{c} - 2r\right)\sin\frac{cs}{2n}$ can be linearized both proximal part and distal part as $\begin{cases} l_{i,p} = m_p \boldsymbol{c_p} + b_p \\ l_{i,d} = m_d \boldsymbol{c_d} + b_d \end{cases}$. So an equation of $l_{i,p}$ and $l_{i,d}$ is

$$l_{i,p} - \frac{m_p}{m_d}\frac{\mathrm{k_d}}{\mathrm{k_p}} l_{i,d} = b_p - \frac{m_p}{m_d}\frac{\mathrm{k_d}}{\mathrm{k_p}} b_d \tag{6}$$

In above equation, each lope and intercept are $m_p = \frac{s_p - l_{i,p}(0.16)}{0-0.16}$, $m_d = \frac{s_d - l_{i,d}(0.16)}{0-0.16}$, $b_p = s_p$, $b_d = s_d$.

Also the equation which is expressed by the relationship of the pulled wire and wire length of the compressed part is

$$n_p l_{i,p} + n_d l_{i,d} = s - l_{i,pull} - \{(t_d \times n) + t_{tip}\} \tag{7}$$

In here, n_p, n_d are the number of proximal and distal part nodes ($n = n_p + n_d$).

So the wire length of the compressed part of spring in proximal and distal part is

$$\begin{bmatrix} l_{i,p} \\ l_{i,d} \end{bmatrix} = \begin{bmatrix} 1 & -\frac{m_p}{m_d}\frac{\mathrm{k_d}}{\mathrm{k_p}} \\ n_p & n_d \end{bmatrix}^{-1} \begin{bmatrix} b_p - \frac{m_p}{m_d}\frac{\mathrm{k_d}}{\mathrm{k_p}} b_d \\ s - l_{i,pull} - \{(t_d \times n) + t_{tip}\} \end{bmatrix}$$

By using the wire lengths, we can get c_p, c_d, ϕ that the first relationship of kinematics for the flexible robot. We add the appendix to explain the wire length of the compressed part for using various springs to get various curvatures.

3.1.4 Calculate the curvature and the angle of curvature ϕ by two adjacent wire

The continuum flexible robot can have infinite angle of curvature with same curvature. The angle of curvature ϕ appears commonly by combination of two orthogonal wires though (1) represents bending to particular orthogonal direction. Figure 12 shows the lateral cross-section when the robot bend to arbitrary direction by l_i, l_{i+1}. In this case we use $\frac{1}{c} - (r + a)$ rather than $\frac{1}{c} - 2r$ for the law of cosine in (1).

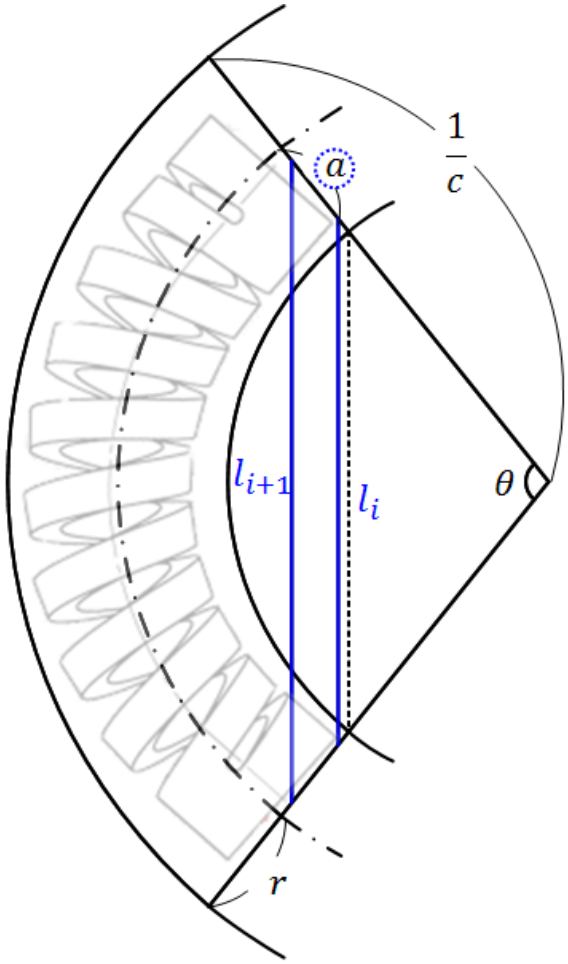

Figure 12. The lateral view of a single sp ring section at the flexible part when two wires were pulled.

In (1), $\frac{1}{c}-2r$ represents the distance of wire from the outer diameter. When the two orthogonal wires are pulled at the same time, we have to reconsider $\frac{1}{c}-2r$ as the Figure 12 shown. In the axial cross section to get an a as the Figure 13 shows, we assume the each direction of wire 1 and 2 from center is positive *x*-direction and *y*-direction. In Figure 13, the robot bend with curvature radius $\frac{1}{c}$ with the angle of curvature ϕ. So we can achieve $a = r\cos\phi$. In the same way, the wire length of compression side when the robot bend with arbitrary angle is

$$l_1 = 2n\left(\frac{1}{c}-r(1+\cos\phi)\right)\sin\frac{cs}{2n},\ l_2 = 2n\left(\frac{1}{c}-r(1+\sin\phi)\right)\sin\frac{cs}{2n} \quad (8)$$

$$l_3 = 2n\left(\frac{1}{c}-r(1-\cos\phi)\right)\sin\frac{cs}{2n},\ l_4 = 2n\left(\frac{1}{c}-r(1-\sin\phi)\right)\sin\frac{cs}{2n}. \quad (9)$$

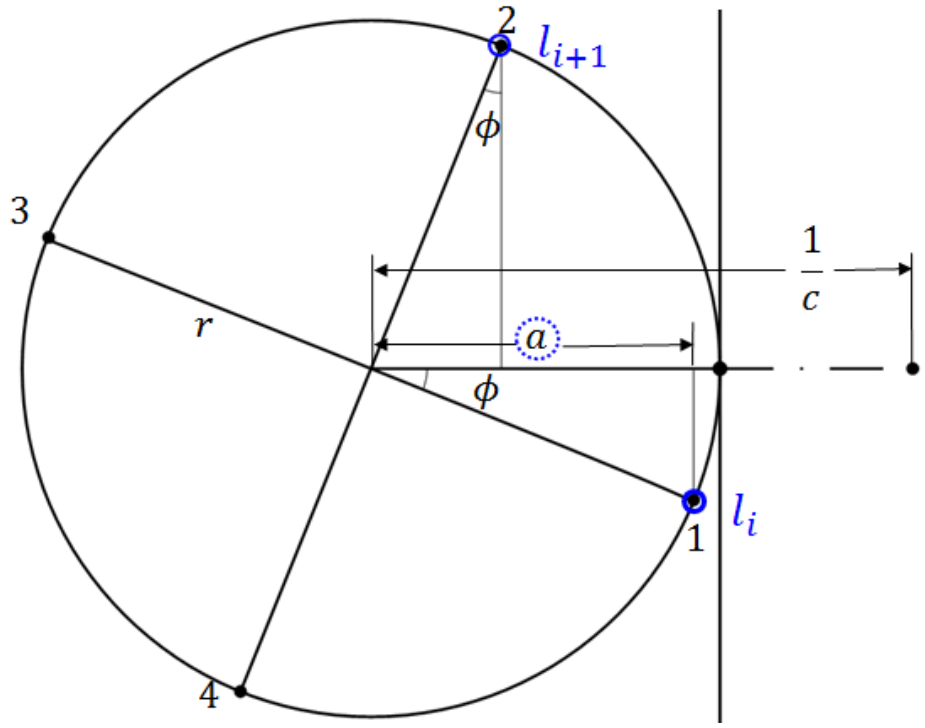

Figure 13. The axial cross-section when two wires were pulled.

To get a function of the wire length, we assume the flexible robot is perfect continuum flexible robot. The equation can be linearized to $l_i = \lim_{n\to\infty} 2n\left(\frac{1}{c} - (r+a)\right)\sin\frac{cs}{2n} = s(1-c(r+a))$. So the c and ϕ are

$$\begin{cases} \phi_{i,i+1} = \tan^{-1}\dfrac{s(1-cr)-l_{i+1}}{s(1-cr)-l_i} \ (when\ wire\ 1{,}2\ or\ 3{,}4\ are\ pulled) \\ \phi_{i,i+1} = -\tan^{-1}\dfrac{s(1-cr)-l_i}{s(1-cr)-l_{i+1}} \ (when\ wire\ 12{,}3\ or\ 4{,}1\ are\ pulled) \end{cases}, c = \frac{s-l_i}{sr\,(1+a_i)} \qquad (10)$$

where, $a_1 = cos\,\phi\,, a_2 = sin\,\phi\,, a_3 = -cos\,\phi\,, a_4 = -\sin\phi$).

3.2 Relationship between c_p, c_d, ϕ and θ, d

To match curvature and the angle of curvature for rigid-link arm with two pair of orthogonal revolute joint which is connected by a prismatic joint, we used geometric information of a single node after bending as shown in Figure 14. When a single section bend, $d = 2n\left(\frac{1}{c} - r\right)\sin\frac{cs}{2n}$ is a distance of center from bottom to tip and $\gamma = \frac{\pi}{2} - \frac{sc}{2}$ is an angle between ZY-plane and d. d can be laid down on XY square which has ($\sqrt{d^2 - Y^2}, d\,cos\,\gamma\,cos\,\phi$).

So the θ_1 and θ_2 are

$$\theta_1 = tan^{-1}\frac{Y}{X} = tan^{-1}\frac{d\,cos\,\gamma\,cos\,\phi}{\sqrt{d^2 - Y^2}} = tan^{-1}\frac{d\,cos\,\gamma\,cos\,\phi}{\sqrt{\left(\left(\frac{1}{c} - r\right)sc\right)^2 - (d\,cos\,\gamma\,cos\,\phi)^2}} \tag{11}$$

$$\theta_2 = -\cos^{-1}\frac{\hbar}{X} = -\cos^{-1}\frac{d\sin\gamma}{\sqrt{d^2 - Y^2}} = -\cos^{-1}\frac{d\sin\gamma}{\sqrt{\left(\left(\frac{1}{c} - r\right)sc\right)^2 - (d\cos\gamma\cos\phi)^2}} \tag{12}$$

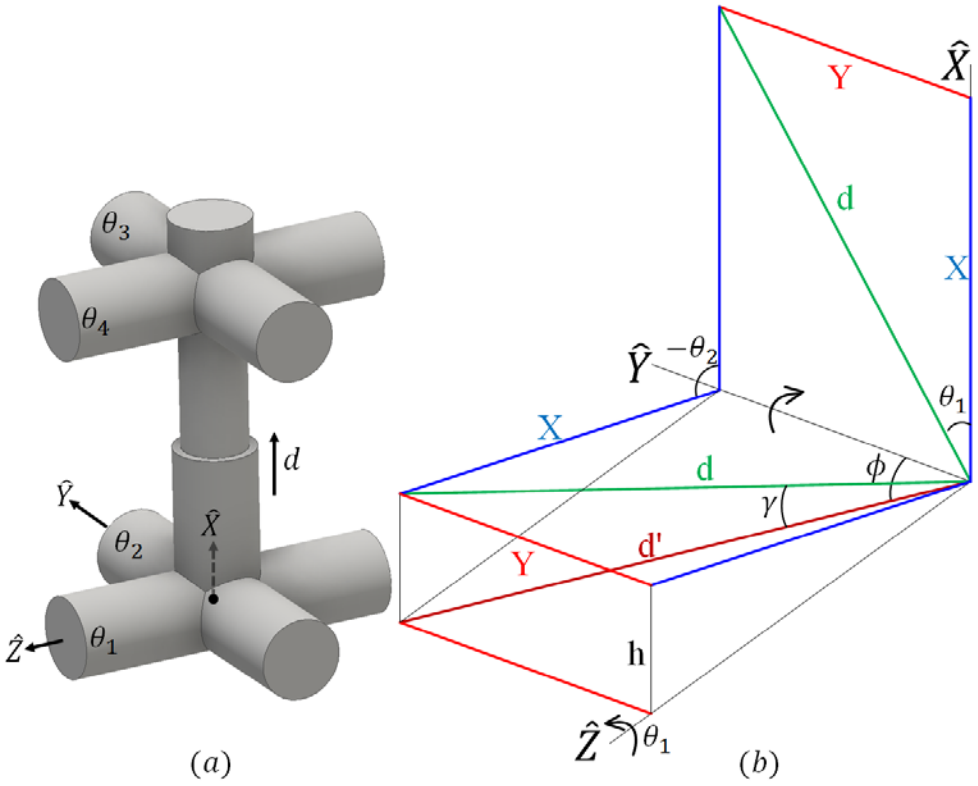

Figure 14. (a) The rigid link-joint model. (b) The geometric information of a single node after bending. The rigid link-joint model lie down on plain XY.

The relationship of revolute joint is $\theta_1 = \theta_4$, $\theta_2 = \theta_3$ because we assume that a node bend symmetry. By prior geometric information, each information of rigid-link arm is

$$\begin{bmatrix}\theta_1\\ \theta_2\\ d\\ \theta_3\\ \theta_4\end{bmatrix} = f_2\left(c,\ \phi\right) = \begin{bmatrix} tan^{-1}\dfrac{d\cos\gamma\cos\phi}{\sqrt{\left(\left(\frac{1}{c}-r\right)sc\right)^2 - d\cos\gamma\cos\phi^2}} \\ -\cos^{-1}\dfrac{d\sin\gamma}{\sqrt{\left(\left(\frac{1}{c}-r\right)sc\right)^2 - (d\cos\gamma\cos\phi)^2}} \\ 2n\left(\frac{1}{c}-r\right)\sin\frac{cs}{2n} \\ -\cos^{-1}\dfrac{d\sin\gamma}{\sqrt{\left(\left(\frac{1}{c}-r\right)sc\right)^2 - (d\cos\gamma\cos\phi)^2}} \\ tan^{-1}\dfrac{d\cos\gamma\cos\phi}{\sqrt{\left(\left(\frac{1}{c}-r\right)sc\right)^2 - d\cos\gamma\cos\phi^2}} \end{bmatrix} \quad (13)$$

3.3 Relationship between c, ϕ and θ, d

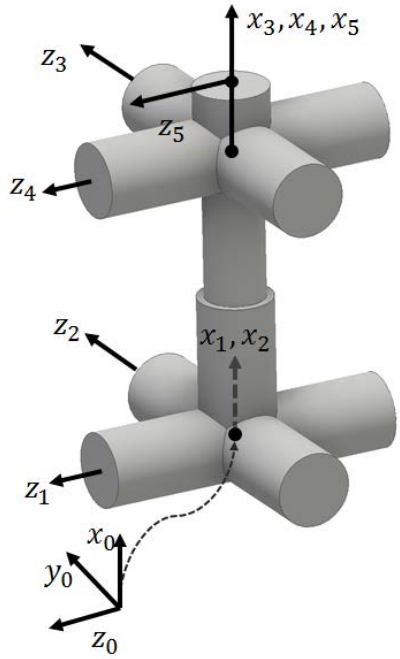

Figure 15. Kinematic representation of the rigid link-joint model for D-H parameters.

To find the coordinate of tip of a segment, rigid-link model was explained by D-H kinematics. In this paper, we use D-H notation which is introduced by [21]. This method yields the D-H table given in Table. 1, illustrated by

Figure 15. In order to calculate the final transformation matrix ${}^{0}_{5}T$, series of matrix multiplications should be carried out.

Table 1. D-H table for rigid-link arm model

	α_{i-1}	a_{i-1}	d_i	θ_i
1	0	0	0	θ_1
2	$-\frac{\pi}{2}$	0	0	θ_2
3	0	d	0	θ_3
4	$\frac{\pi}{2}$	0	0	θ_4
5	0	a	0	0

$$ {}^{0}_{5}T = {}^{0}_{1}T\,{}^{1}_{2}T\,{}^{2}_{3}T\,{}^{3}_{4}T\,{}^{4}_{5}T \tag{14}$$

where,

$$ {}^{0}_{1}T = \begin{bmatrix} \cos\theta_1 & -\sin\theta_1 & 0 & 0 \\ \sin\theta_1 & \cos\theta_1 & 0 & 0 \\ 0 & 0 & 1 & 0 \\ 0 & 0 & 0 & 1 \end{bmatrix}, \quad {}^{1}_{2}T = \begin{bmatrix} \cos\theta_2 & -\sin\theta_2 & 0 & 0 \\ 0 & 0 & 1 & 0 \\ -\sin\theta_2 & -\cos\theta_2 & 0 & 0 \\ 0 & 0 & 0 & 1 \end{bmatrix}, $$

$$ {}^{2}_{3}T = \begin{bmatrix} \cos\theta_3 & -\sin\theta_3 & 0 & 0 \\ \sin\theta_3 & \cos\theta_3 & 0 & 0 \\ 0 & 0 & 1 & 0 \\ 0 & 0 & 0 & 1 \end{bmatrix}, \quad {}^{3}_{4}T = \begin{bmatrix} \cos\theta_4 & -\sin\theta_4 & 0 & 0 \\ 0 & 0 & -1 & 0 \\ \sin\theta_4 & \cos\theta_4 & 0 & 0 \\ 0 & 0 & 0 & 1 \end{bmatrix}, $$

$$ {}^{4}_{5}T = \begin{bmatrix} 1 & 0 & 0 & a \\ 0 & 1 & 0 & 0 \\ 0 & 0 & 1 & 0 \\ 0 & 0 & 0 & 1 \end{bmatrix}. $$

Substituting above matrixes to (14), the result of the homogenous transformation matrix ${}^{0}_{5}T$ is

$$ {}^{0}_{5}T = \begin{bmatrix} u_x & v_x & w_x & p_x \\ u_y & v_y & w_y & p_y \\ u_z & v_z & w_z & p_z \\ 0 & 0 & 0 & 1 \end{bmatrix} \tag{15} $$

where,

$u_x = -s\theta_1 s\theta_4 c\theta_3 + c\theta_1 c\theta_2 c\theta_3 c\theta_4 - c\theta_1 s\theta_2 s\theta_3,$

$u_y = c\theta_1 s\theta_4 c\theta_3 + s\theta_1 c\theta_2 c\theta_3 c\theta_4 + s\theta_1 s\theta_2 s\theta_3,$

$u_z = c\theta_2 c\theta_3 c\theta_4 + c\theta_2 c\theta_3,$

$v_x = s\theta_1 s\theta_3 s\theta_4 - c\theta_1 c\theta_2 c\theta_4 s\theta_3 - c\theta_1 s\theta_2 c\theta_3,$

$v_y = -c\theta_1 s\theta_3 s\theta_4 - s\theta_1 c\theta_2 c\theta_4 s\theta_3 + s\theta_1 s\theta_2 c\theta_3,$

$v_z = -c\theta_2 c\theta_4 s\theta_3 + c\theta_2 c\theta_3,$

$w_x = s\theta_1 c\theta_4 + c\theta_1 c\theta_2 s\theta_4,\ w_y = -c\theta_1 c\theta_4 + s\theta_1 c\theta_2 s\theta_4,\ w_z = s\theta_2 s\theta_4,$

$p_x = au_x + dc\theta_1 c\theta_2,$

$p_y = au_y + ds\theta_1 c\theta_2,$

$p_z = au_z + ds\theta_2,$

$c = cos\,\theta$ and $s = sin\,\theta.$

We can obtain the whole transformation matrix of a flexible robot by multiply ${}^{0}_{5}T$ by the number of springs. Also transformation matrix should be divided according to the kind of springs.

IV. EXPERIMENTS AND RESULTS

1.1 Experiment method

In this experiment, we investigate the mobility of the flexible robot. For evaluate the curvature according to the length of wire pulled, the only one wire was pulled so the robot bent to one side. So the curvature formation angle was fixed to 0. The robot was laid down a graph paper and the wire which is connected to vernier calipers was pulled from $0mm$ to $15mm$ as shown in Figure 16. Every bending state was recorded by camera. To avoid the distortion caused by distance from camera lens to subject (which is the flexible part in this case), the camera was away $400mm$ from graph paper. The horizontality of camera was checked by inclinometer. After taking pictures, we measured the value of every parameters in prior equations by overlapped the taken pictures on the CAD (Inventor, Autodesk) then the taken sixteen pictures are resized in CAD to real size. Figure 17 shows two examples of measured pictures.

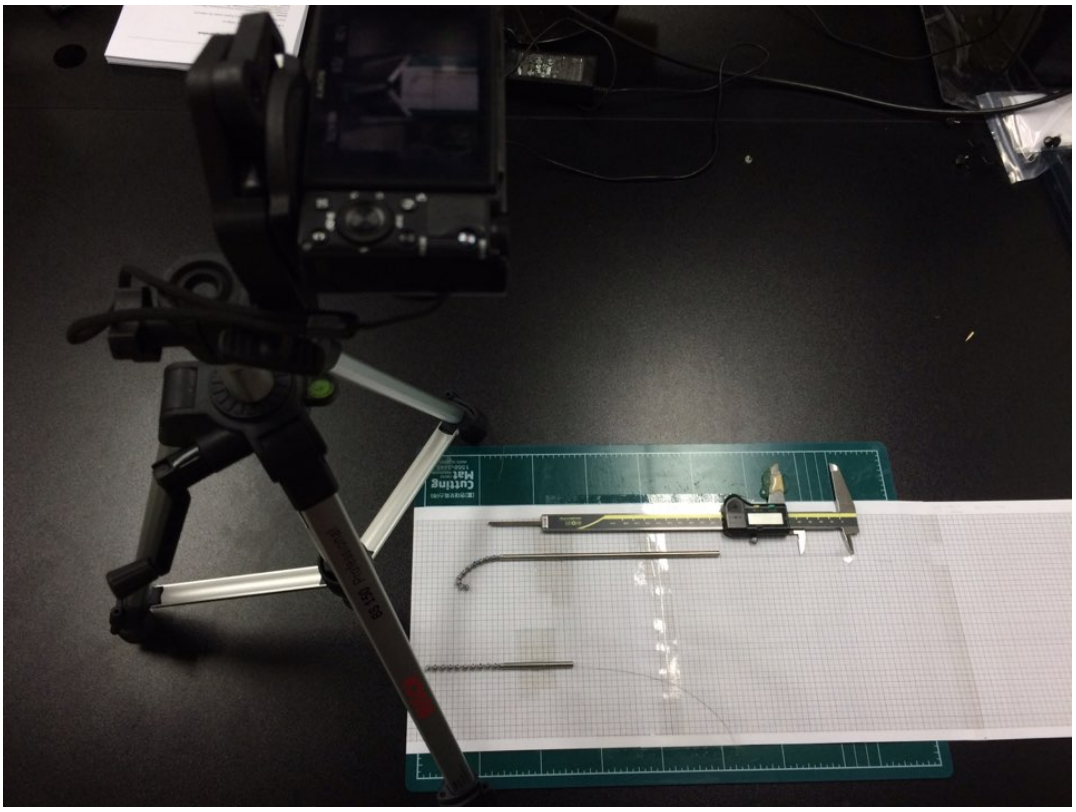

Figure 16. The experiment environment for measuring curvatures and positions.

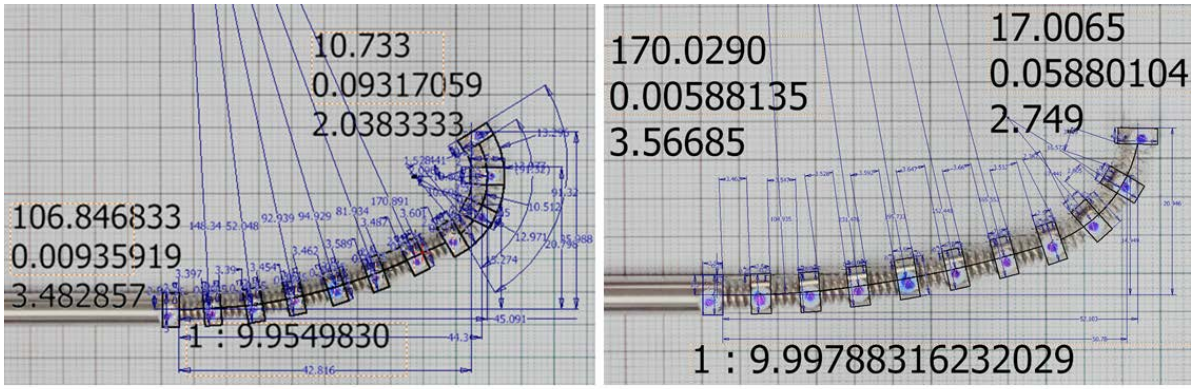

(a) (b)

Figure 17. The example about measuring method for curvatures, positions and curvature ratios.

1.2 Comparing estimated value and measured value

The curvature variation of continuum flexible robot evaluated by comparing estimated value and measured value. In Figure 18, we compare curvature of proximal and distal part. In this case estimated value and measured value was almost same because the tendency was almost equal both part. The graph's slope of real value was 9 rather than 10 which was expected value.

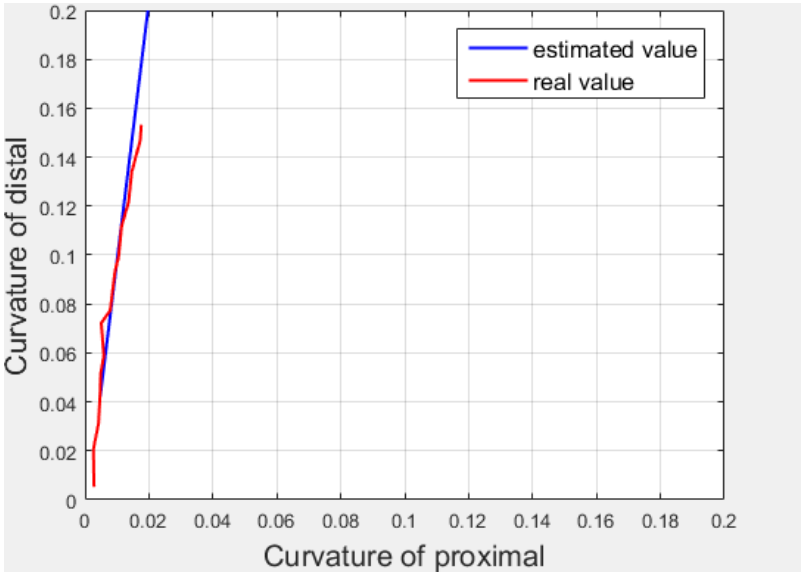

Figure 18. Comparing proximal and distal curvatures.

The Figure 19 shows the curvature ratio convergent to 9 in both estimated value and real value. It has same

meaning with Figure 18.

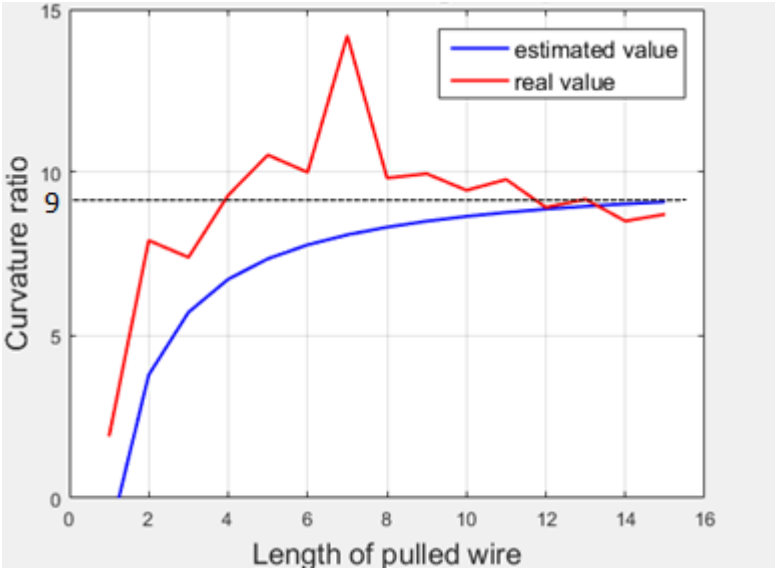

Figure 19. Curvature ratio and length of pulled wire

In Figure 20, we compare wire length of compression side at proximal and distal part. As we checked from prior result which is curvature and wire length, the error increases as the both part of wire getting shorter.

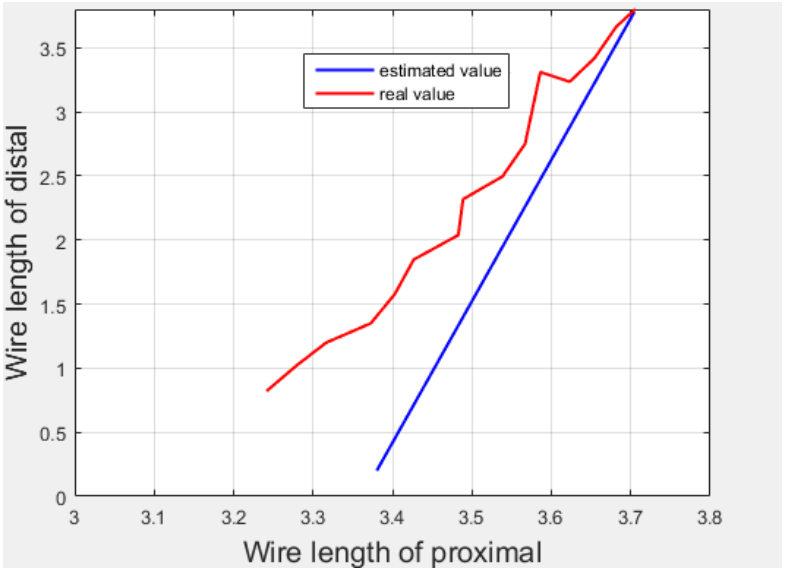

Figure 20. Comparing proximal and distal wire lengths of compression side.

In Figure 21, we evaluate the curvature and line length of compressed side. Both proximal and distal value of

real and estimated value has same tendency. In distal part, the largest error was 0.287mm at curvature is $0.1217mm^{-1}$. In proximal part, the largest error was 0.164mm at curvature is $0.0177mm^{-1}$. The error gets bigger as the wire length becoming shorter.

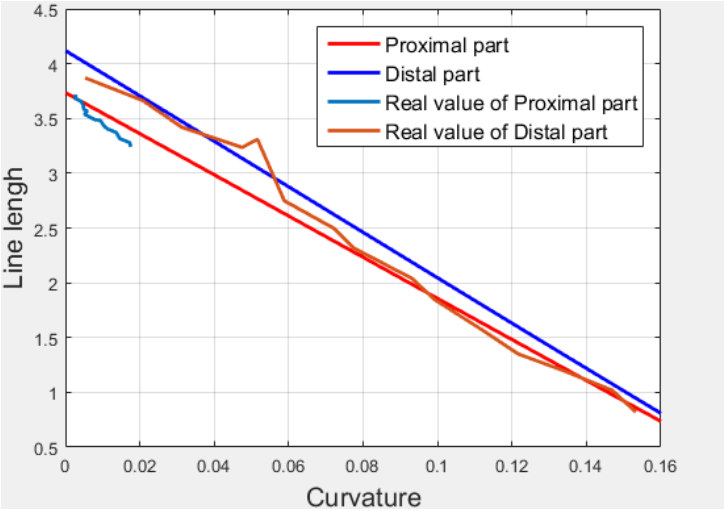

Figure 21. Relationship between line length l_i and curvature c in proximal and distal part in the flexible part.

In Figure 22, we evaluate the position at X-Y plane through the transformation matrix of (15). As the robot bent more, the estimated value was not well fitted with real value. Real trajectory tends to bent more than estimated value. It caused by line length of measured value gets shorter as the curvature gets larger. Due to accumulate of error, position error occurs.

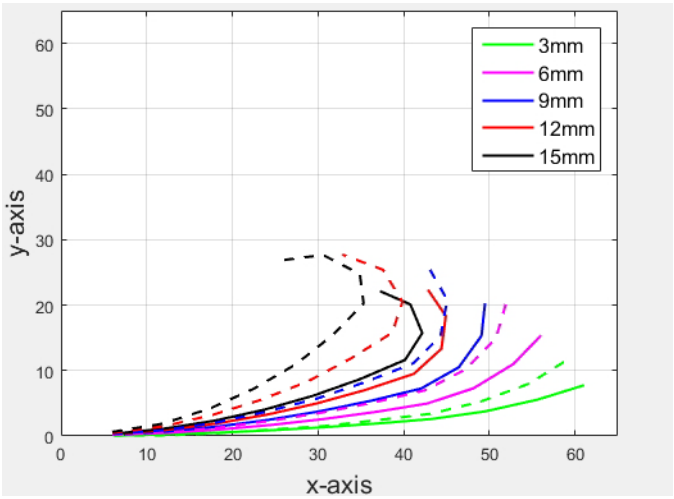

Figure 22. Position at X-Y plane. The solid-line is estimated value and dotted-line is real value.

1.3 Phantom experiment of the larger curvature at the tip and conventional flexible robot

In this research, we designed the continuum flexible robot with larger curvature at the tip. As we said in 1.1, the continuum flexible robot has to have larger curvature at the tip for the orbital floor blowout surgery. The phantom experiment was executed to evaluate the effectiveness for the using at surgery. The flexible robot has to pass through narrow and highly curved path. The phantom was made by 3D printer (Objet ADEN E250, Stratasys) and its shape resemble human nasal path which is from nostril to maxillary sinus. The phantom expose the cross-section of path for checking robot's movement inside of the phantom. The proposed continuum flexible robot can go through the narrow space as shown in Figure 23. Beside the proposed continuum flexible robot can reach a goal location, the continuum flexible robot which has same springs stuck by inner entrance of goal location. Because the comparison robot cannot highly bend in front of the inner entrance. When the comparison robot was pushed harder as shown in Figure 23 (b), only body of the comparison robot bent more while the proposed continuum flexible robot go through the path smoothly.

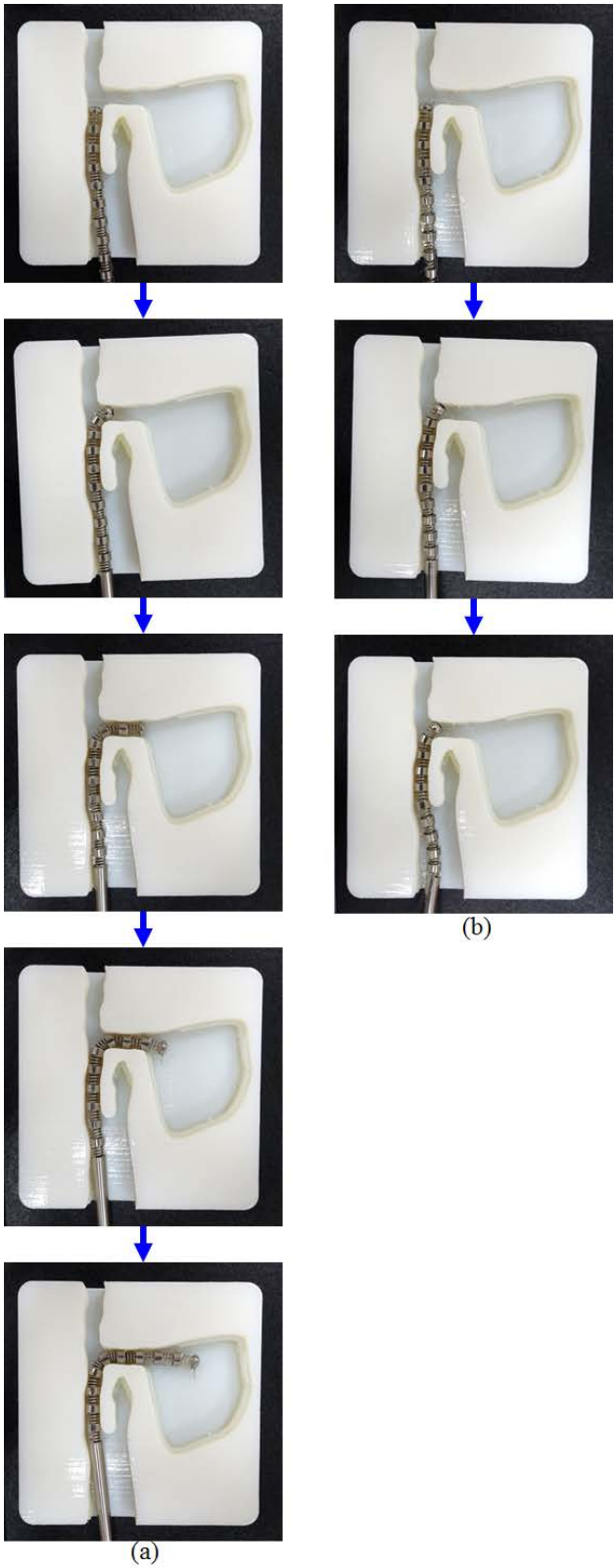

Figure 23. Comparison of work performance between the larger curvature continuum flexible robot and the robot which has same springs. (a) is the continuum flexible robot with larger curvature at the tip and (b) is the continuum flexible robot which has same springs.

V. DISCUSSION AND CONCLUSIONS

In this paper, a continuum flexible robot with multiple curvature has been developed and evaluated curvature changes in respect to length of wire pulled. The orbital floor blowout surgery of transnasal and transconjunctival approach was motivated about the research subject. In transnasal approach, a flexible robot which can control the curvature was needed. Due to narrow and sharply curved structure of transnasal pathway, the tip of flexible robot must has larger curvature than other section. Because it is hard to get into the sharply curved pathway if the flexible robot has constant curvature. So we suggested the continuum flexible robot which has larger curvature at the tip.

We made the $5mm$ outer diameter flexible robot with ten $4mm$ outer diameter compression springs as prototype. From base to seventh spring has ten times larger than rest three springs. First of all, we analyzed and evaluated with assuming the flexible robot has equal curvature at the same spring. The robot has larger curvature as the wire length shorten when we compared with estimated value. It has two major causes.

First, it caused by choosing neutral arc at (1). This problem come from analysis of kinematics. When the spring get eccentric pressure from wire for bending, we assumed the outer arc of Figure 8 has constant length. But strictly speaking, the position of neutral arc always change depending on the length of the compressed side of wire. Outer arc also shorten when the wire is shorten not much. But when the wire is shorten much, the flexible robot has larger curvature and it influence to lower spring by the form of moment. So the neutral arc move to between outer arc and middle arc. We can checked it by putting $(\frac{1}{c} - 1.47r)$ when we using the law of cosine at (1). The modified result was better fitted than prior result. When we put $r = 1.5$ rather than $r = 2.5$ as Figure 24 shown, the position error of the continuum flexible robot was reduced. For the future work, finding proper r at each curvature is needed. Until this research, we can increase the accuracy of estimated value of the continuum flexible robot's position data through getting accurate location of neutral arc in Figure 8 at each bending angle. Then we put the each r values in case by case. In the future work, we need the proper relationships of bending angle with change of r which express the location of neutral arc.

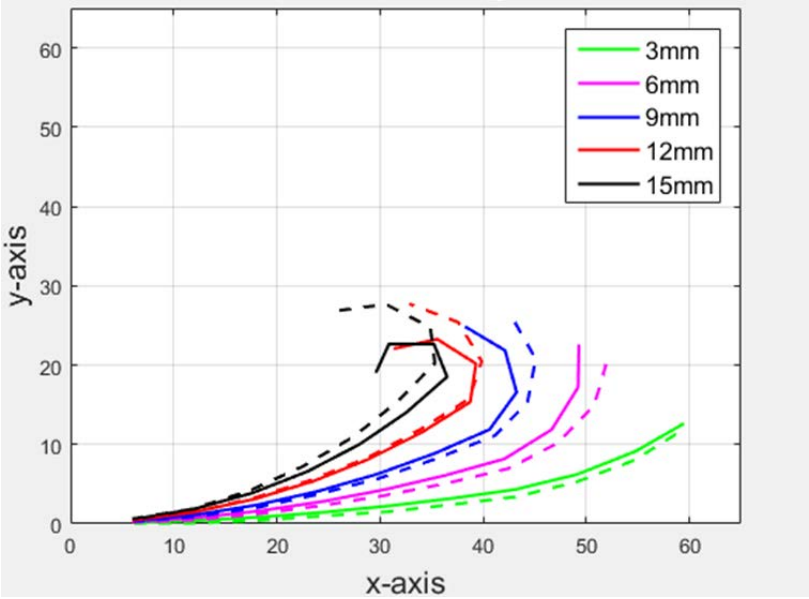

Figure 24. Position at X-Y plane when r is 1.5 rather than 2.5. The legend mean the pulled length of wire. The solid-line is estimated value and dotted-line is real value.

Second is friction between wire and cylinder [12], [13], [22]. This problem is kind of kinetics. As we can watched by Figure 25 which has same springs throughout the flexible robot, springs has larger curvature as it goes to the conduit. This phenomenon is also appeared more prominent at the tip of the multiple curvature flexible robot. Even if we modified the value of the distance of neutral arc line, the error of the position was larger as the curvature increased. Also there are mechanical errors which is possibility of differences in the number of active (or effective) coils at each section due to adhesion method of springs.

In experiment, we measured and compared only curvatures and position data. We cannot measured the angle of curvature ϕ due to some reasons. To measure a 3D position data, we try to use optical tracking systems (Polaris, NDI) with markers, 3D camera (Intel® Realsense™) and 3D scanner (Artec Spider). When we try to use optical tracking systems, it was hard to get position data without the continuum flexible robot's deflection. We have to touch to the continuum flexible robot with probe which is attached markers. We also cannot get 3D position data because the continuum flexible robot has gloss surface. Both devices have to receive light refection so the devices cannot detect the surface of the continuum flexible robot. [23], [24] shows research about tracking the flexible robots. For the future work, we can achieve position data through changing the material or modifying the measuring system of the continuum flexible robot.

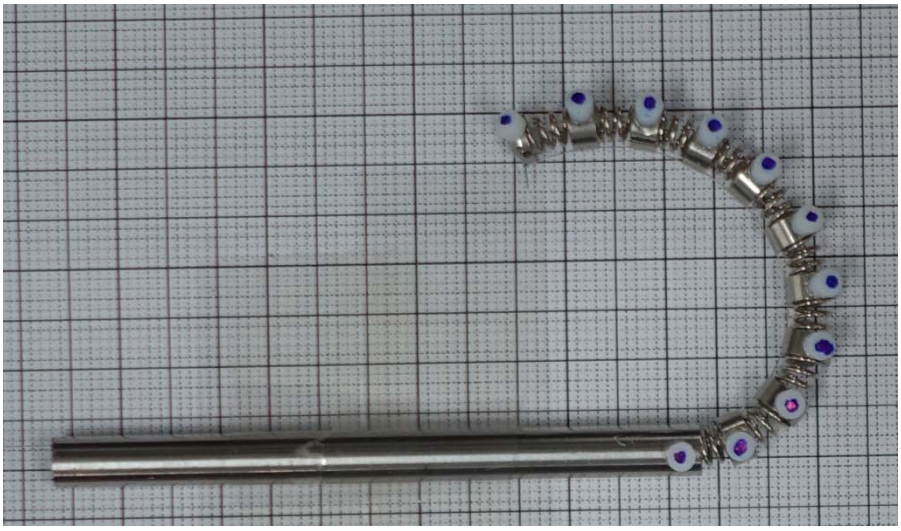

Figure 25. The comparison test of the flexible robot which is composed of equal springs.

This paper formulate the method and model of the continuum flexible robot. As the flexible robot bent much, the error increased. The ratio of curvature is more important than robot's position data as shown in Figure 23. Because the continuum flexible robot go through the narrow path by its natural mechanical backdrivability. The ratio of curvature which express the possibility of moving to side path in forked road should be guaranteed. So guarantee of the expected curvature is more important than the position data of the continuum flexible robot. The movement of tendency was followed well but kinematic problem of neutral arc location which is also related with mechanical analysis of compression spring should be modified. The mechanical friction between wire and cylinder should be considered additionally. If this problems solve at future study, the analysis of the continuum flexible robot will be more precise. Also we need feedbacks from doctors for more information of the orbital floor blowout surgery. We need the exact required curvatures, convenience of operation, maximum diameter of flexible robot etc.

References

[1] J. H. Ahn and S. G. Lee, "A Case of Anti-GQ1b-Positive atypical Miller Fisher syndrome with pupil involvement," *Journal of the Korean Ophthalmological Society,* vol. 50, pp. 645-648, 2009.

[2] M. Kakibuchi, K. Fukazawa, K. Fukuda, N. Yamada, K. Matsuda, K. Kawai*, et al.*, "Combination of transconjunctival and endonasal-transantral approach in the repair of blowout fractures involving the orbital floor," *British journal of plastic surgery,* vol. 57, pp. 37-44, 2004.

[3] W. Tasman and E. A. Jaeger, *The Wills Eye Hospital atlas of clinical ophthalmology*: Lippincott Williams & Wilkins, 2001.

[4] Dom1953. (2014). *Diplopia and Central Vision Suppression*. Available: https://upload.wikimedia.org/wikipedia/commons/thumb/e/e8/Figure_of_diplopia_perception_with_English_annotations.svg/873px-Figure_of_diplopia_perception_with_English_annotations.svg.png

[5] N. M. A. D. Stock, "Fractured Eye Socket - Or;bital Fracture Reconstruction Surgery," ed, 2012.

[6] N. K. Lim, D. H. Kang, S. A. Oh, and J. H. Gu, "Orbital Floor Restoration Using the Transnasal Balloon Technique for Inferior Orbital Wall Fracture," *Annals of plastic surgery,* vol. 75, pp. 522-525, 2015.

[7] M. W. Hannan and I. D. Walker, "Kinematics and the implementation of an elephant's trunk manipulator and other continuum style robots," *Journal of Robotic Systems,* vol. 20, pp. 45-63, 2003.

[8] B. A. Jones and I. D. Walker, "Kinematics for multisection continuum robots," *Robotics, IEEE Transactions on,* vol. 22, pp. 43-55, 2006.

[9] D. Trivedi, C. D. Rahn, W. M. Kier, and I. D. Walker, "Soft robotics: Biological inspiration, state of the art, and future research," *Applied Bionics and Biomechanics,* vol. 5, pp. 99-117, 2008.

[10] I. D. Walker, "Continuous backbone "continuum" robot manipulators," *ISRN Robotics,* vol. 2013, 2013.

[11] D. B. Camarillo, C. F. Milne, C. R. Carlson, M. R. Zinn, and J. K. Salisbury, "Mechanics modeling of tendon-driven continuum manipulators," *Robotics, IEEE Transactions on,* vol. 24, pp. 1262-1273, 2008.

[12] J. Jung, R. S. Penning, N. J. Ferrier, and M. R. Zinn, "A modeling approach for continuum robotic manipulators: effects of nonlinear internal device friction," in *Intelligent Robots and Systems (IROS), 2011 IEEE/RSJ International Conference on*, 2011, pp. 5139-5146.

[13] G. Subramani and M. R. Zinn, "Tackling friction-an analytical modeling approach to understanding friction in single tendon driven continuum manipulators," in *Robotics and Automation (ICRA), 2015 IEEE International Conference on*, 2015, pp. 610-617.

[14] W. S. Rone and P. Ben-Tzvi, "Continuum robot dynamics utilizing the principle of virtual power," *Robotics, IEEE Transactions on,* vol. 30, pp. 275-287, 2014.

[15] C. Laschi, M. Cianchetti, B. Mazzolai, L. Margheri, M. Follador, and P. Dario, "Soft robot arm

inspired by the octopus," *Advanced Robotics,* vol. 26, pp. 709-727, 2012.

[16] H.-S. Yoon, S. M. Oh, J. H. Jeong, S. H. Lee, K. Tae, K.-C. Koh*, et al.*, "Active bending endoscope robot system for navigation through sinus area," in *Intelligent Robots and Systems (IROS), 2011 IEEE/RSJ International Conference on*, 2011, pp. 967-972.

[17] H.-S. Yoon, H.-J. Cha, J. Chung, and B.-J. Yi, "Compact design of a dual master-slave system for maxillary sinus surgery," in *Intelligent Robots and Systems (IROS), 2013 IEEE/RSJ International Conference on*, 2013, pp. 5027-5032.

[18] R. D. Zheng Li, "Design and Analysis of a Bio-Inspired Wire-Driven Multi-Section Flexible Robot," *International Journal of Advanced Robotic Systems,* 2013.

[19] R. D. Zheng Li, Haoyong Yu and Hongliang Ren, "Statics Modeling of an Underactuated Wire-Driven Flexible Robotic Arm," in *IEEE RAS & EMBS International Conference on Biomedical Robotics and Biomechatronics (BioRob)*, São Paulo, Brazil, 2014.

[20] A. M. Wahl, *Mechanical springs*: Penton Publishing Company, 1944.

[21] J. J. Craig, *Introduction to robotics: mechanics and control* vol. 3: Pearson Prentice Hall Upper Saddle River, 2005.

[22] B. Kaewkham-ai and K. Uthaichana, "Comparative study on friction compensation using Coulomb and Dahl models with extended and unscented Kalman filters," in *Industrial Electronics and Applications (ICIEA), 2012 7th IEEE Conference on*, 2012, pp. 191-195.

[23] D. B. Camarillo, K. E. Loewke, C. R. Carlson, and J. K. Salisbury, "Vision based 3-D shape sensing of flexible manipulators," in *Robotics and Automation, 2008. ICRA 2008. IEEE International Conference on*, 2008, pp. 2940-2947.

[24] Y. Shapiro, G. Kósa, and A. Wolf, "Shape tracking of planar hyper-flexible beams via embedded PVDF deflection sensors," *IEEE/ASME Transactions on Mechatronics,* vol. 19, pp. 1260-1267, 2014.

요약문

여러 곡률을 갖는 연속체로 이루어진 휘어지는 로봇

연속체로 된 휘어지는 로봇들은 기존의 강체로 이루어진 로봇에 비해 유연한 특성을 갖기 때문에 여러 가지 분야에서 사용된다. 많은 적용분야 중 본 논문은 ballooning 안와하골절 수술 분야에 적용될 수 있는 continuum flexible robot에 대하여 연구했다. 안와하골절은 매우 빈번하게 일어나는 외상으로써, 골절부위를 풍선으로 받쳐주면 수술의 완성도를 높일 수 있지만 숙달된 소수의 의사만 집도 가능하다는 단점이 있다. 가장 핵심적인 문제는 로봇이 한 자유도 방향으로 움직일 때 로봇의 끝 부분이 급격하게 구부러져야 한다는 것이다. 기존의 연속체로 된 휘어지는 로봇들은 가정 또는 기구적인 구속을 통해 전체적으로 일정한 곡률을 갖도록 만들거나 와이어로 연결된 엑추에이터들의 숫자를 늘려서 자유도를 증가시키는 접근법을 보여주었다. 이러한 단점들을 보완하기 위해 본 논문에서는 엑추에이터의 숫자를 늘리지 않으면서 끝 부분의 곡률이 더 클 수 있는 연속체로 된 휘어지는 로봇을 설계하고 사용한 스프링 상수에 따른 곡률 비, 당겨진 와이어 길이에 따른 곡률, 기구학 등을 분석했다. 만들어진 로봇의 와이어를 $0mm$~$15mm$ 만큼 당겨서 곡률 비와 부분별 곡률을 측정하고 분석하여 나온 식과 대응 값을 적용시킨 시뮬레이션을 통해 성능평가를 실시하였다.

핵심어 : 연속체로 된 휘어지는 로봇, 곡률, 곡류 비, 기구학

APPENDIX

The continuum flexible robot can be used more than 2 springs. This means the wire length of the compressed part of spring can be divided by 3 parts or more. In 3.1.3, we calculated only two parts which are proximal part $l_{i,p}$ and distal part $l_{i,d}$. We have to prove the method of 3.1.3 to apply in using various springs. First we calculated the wire length of the compressed part of three springs. Suppose the ratio of spring constant is $k_1 : k_2 : k_3 = 4 : 2 : 1$ and each ratio of slope which is achieved by equation (1) is $\frac{m_{i-1}}{m_i} = 1$. We can get the three equations of two linearized graph equations and the relationship of the pulled wire and wire length of the compressed part.

$$\begin{cases} l_1 - 0.5l_2 = b_1 - 0.5b_2 \\ l_2 - 0.5l_3 = b_2 - 0.5b_3 \\ n_1 l_1 + n_2 l_2 + n_3 l_3 = s - l_{i,pull} - \{(t_d \times n) + t_{tip}\} \end{cases}$$

We can express above equations by matrixes.

$$\begin{bmatrix} 1 & -0.5 & 0 \\ 0 & 1 & -0.5 \\ \mathrm{n}_1 & \mathrm{n}_2 & \mathrm{n}_3 \end{bmatrix} \begin{pmatrix} l_1 \\ l_2 \\ l_3 \end{pmatrix} = \begin{bmatrix} b_1 - 0.5b_2 \\ b_2 - 0.5b_3 \\ s - l_{i,pull} - \{(t_d \times n) + t_{tip}\} \end{bmatrix}$$

$$\boldsymbol{Al} = \boldsymbol{B}$$

$$\therefore \boldsymbol{l} = \boldsymbol{A^{-1}B}$$

The matrix $\boldsymbol{A}$ is nonsingular matrix by checking $det(\boldsymbol{A})$.

When we increase the dimension of vectors and matrixes, vector of wire lengths of the compressed part of springs can be expressed by matrix $\boldsymbol{A}_{n\times n}$ and vector $\boldsymbol{B}_{n\times 1}$. So the final equation of the wire length of the compressed part is

$$\boldsymbol{l}_{n\times 1} = {\boldsymbol{A}_{n\times n}}^{-1}\boldsymbol{B}_{n\times 1}.$$

Where,

$$\begin{pmatrix} l_1 \\ l_2 \\ l_3 \\ \vdots \\ l_n \end{pmatrix} = \boldsymbol{l}_{n\times 1},\ \begin{bmatrix} 1 & -\frac{m_1}{m_2}\frac{k_2}{k_1} & 0 & \cdots & \cdots & 0 \\ 0 & 1 & -\frac{m_2}{m_3}\frac{k_3}{k_2} & \cdots & \cdots & 0 \\ \vdots & \vdots & 1 & -\frac{m_3}{m_4}\frac{k_4}{k_3} & \cdots & 0 \\ \vdots & \vdots & \vdots & \vdots & \ddots & \vdots \\ n_1 & n_2 & n_3 & \cdots & \cdots & n_n \end{bmatrix} = \boldsymbol{A}_{n\times n},\ \begin{bmatrix} b_1 - \frac{m_1}{m_2}\frac{k_2}{k_1}b_2 \\ b_2 - \frac{m_2}{m_3}\frac{k_3}{k_2}b_3 \\ b_3 - \frac{m_3}{m_4}\frac{k_4}{k_3}b_4 \\ \vdots \\ b_{n-1} - \frac{m_{n-1}}{m_n}\frac{k_n}{k_{n-1}}b_n \\ s - l_{i,pull} - \{(t_d \times n) + t_{tip}\} \end{bmatrix} = \boldsymbol{B}_{n\times 1}$$